



## Heterogeneously degradation of aniline in aqueous solution using persulfate catalyzed by magnetic BiFeO<sub>3</sub> nanoparticles

Imtyaz Hussain<sup>a,b,c,\*</sup>, Yongqing Zhang<sup>c,d,e,\*</sup>, Mingyu Li<sup>a,b,\*\*</sup>, Shaobin Huang<sup>c,d,e</sup>, Waseem Hayat<sup>c</sup>, Liangming He<sup>b</sup>, Xiaodong Du<sup>c</sup>, Guoqiang Liu<sup>a,b</sup>, Meimei Du<sup>c</sup>

<sup>a</sup> The Research Center of Water Treatment Technique and Material Engineering, Jinan University, Guangzhou, Guangdong Province, PR China

<sup>b</sup> School of Environment, Jinan University, Guangzhou 510632, PR China

<sup>c</sup> School of Environment and Energy, Guangdong Provincial Key Laboratory of Atmospheric Environment and Pollution Control, South China University of Technology, Guangzhou, 510006, PR China

<sup>d</sup> State Key Laboratory of Pulp and Paper Engineering, South China University of Technology, Guangzhou, 510640, PR China

<sup>e</sup> The Key Lab of Pollution Control and Ecosystem Restoration in Industry Clusters, Ministry of Education, Guangzhou 510006, PR China

### ARTICLE INFO

#### Keywords:

BFO MNPs  
AOPs  
Sulfate radicals  
Hydroxyl radicals  
Aniline  
Degradation

### ABSTRACT

In this study, magnetic BiFeO<sub>3</sub> nanoparticles (BFO MNPs) were successfully synthesized by simple sole-gel method. The BFO MNPs catalyst was characterized by X-ray diffraction (XRD), scanning electron microscopy (SEM), energy-dispersive spectroscopy (EDS), x-ray photoelectron spectroscopy (XPS) and Fourier transform infrared (FT-IR) techniques. The prepared catalyst was used to activate persulfate (PS) to generate sulfate radicals (SO<sub>4</sub>·<sup>-</sup>) for the enhanced degradation of aniline from aqueous solution. It was found that BFO MNPs showed high catalytic activity toward PS decomposition for the degradation of aniline. The degradation efficiency of aniline (0.5 mM) was 100% within 120 min using initial dosage of 0.5 g/L BFO MNPs and concentration of 5 mM persulfate. Even at neutral pH (7.0), aniline was efficiently degraded in BFO MNPs /PS system. The effects of reaction parameters such as initial pH, PS concentration and dosage of BFO MNPs were investigated. The radical scavenging and electron paramagnetic resonance (EPR) results showed that sulfate radicals (SO<sub>4</sub>·<sup>-</sup>) and hydroxyl radicals (·OH) were generated by the activation of PS with BFO MNPs for the degradation of aniline. The stability of catalyst was tested by means of successive reuse cycles. The results revealed that BiFeO<sub>3</sub> catalyst exhibited high reusability and stability in degrading aniline through PS activation.

### 1. Introduction

Organic contaminants are continuously being released into the environment with rapid development of industrialization and urbanization. Among the toxic contaminants present in wastewater, aniline is a toxic compound widely used as an intermediate in the synthesis of pharmaceuticals, dyes, antioxidants, polyurethanes, rubber additives, pesticides and herbicides [1]. The annual estimation discharge of aniline into the environment is 30,000 tons by illegal discharge of municipal and industrial wastewater, excessive pesticides use and accidental leakages [2]. Aniline is injurious to the human beings and aquatic life because it is bio-refractory, mutagenic, carcinogenic, toxic and potentially fatal. It has been listed as one of the 129 priority pollutants by the U.S Environmental Protection Agency (U.S.EPA) [3,4]. Therefore, novel and effective method is necessary to degrade aniline in aqueous

solution.

Advanced oxidation processes (AOPs) for the treatment of wastewater have received growing attention as effective and attractive pathways due to generation of highly reactive species in these processes [5]. Among AOPs, classic Fenton process is commonly used due to its capacity to degrade organic compounds. However, classic Fenton process (Fe<sup>2+</sup>/H<sub>2</sub>O<sub>2</sub>) has certain restrictions such as requiring lower pH (pH < 3.0), formation of sludge residues, and unsuccessful use of rapidly produced hydroxyl radicals and limited elimination of organic carbon [6]. Recently, oxidation with sulfate radical (SO<sub>4</sub>·<sup>-</sup>) from PS is proved as promising and efficient pathway due to its ability to degrade organic pollutants into non-toxic small molecule substances [7–10]. Compared to ·OH, which has redox potential of 1.8–2.7 V, SO<sub>4</sub>·<sup>-</sup> exhibits a higher redox potential of 2.5–3.1 V. SO<sub>4</sub>·<sup>-</sup> reacts with wide range of organic contaminants through a one-electron transfer

\* Corresponding authors at: School of Environment and Energy, Guangdong Provincial Key Laboratory of Atmospheric Environment and Pollution Control, South China University of Technology, Guangzhou, 510006, PR China.

\*\* Corresponding author at: The Research Center of Water Treatment Technique and Material Engineering, Jinan University, Guangzhou, Guangdong Province, PR China.  
E-mail addresses: [imtiazauf@yahoo.com](mailto:imtiazauf@yahoo.com) (I. Hussain), [zhangyq@scut.edu.cn](mailto:zhangyq@scut.edu.cn) (Y. Zhang), [limingyu2000@163.com](mailto:limingyu2000@163.com) (M. Li).

<https://doi.org/10.1016/j.cattod.2018.02.017>

Received 23 May 2017; Received in revised form 27 November 2017; Accepted 12 February 2018

Available online 13 February 2018

0920-5861/ © 2018 Elsevier B.V. All rights reserved.

mechanism while  $\cdot\text{OH}$  reacts by hydrogen abstraction or addition reaction [11].  $\text{SO}_4\cdot^-$  has longer half-life, strong oxidizing ability, and higher reactivity over wide pH [12,13]. Furthermore,  $\text{SO}_4\cdot^-$  is relatively stable and quickly react with the organic pollutants with second order rate constants ranging from  $10^7$ – $10^9 \text{ M}^{-1} \text{ s}^{-1}$  [14]. Mostly,  $\text{SO}_4\cdot^-$  can be generated by the activation of PS through heat [3,15], UV light [16], transition metals [17,18], electron transfer and base (Eqs (1)–(3)) [19]. Once  $\text{SO}_4\cdot^-$  is produced, hydroxyl radical can be formed indirectly (Eqs. (4), (5)) [7], which also contributes to the degradation of pollutants [14].



( $\text{M}^{n+} = \text{Ag}^+, \text{Cu}^+, \text{Co}^{2+}, \text{Fe}^{2+}, \text{Ce}^{3+}, \text{Mn}^{2+}$ , etc)

Among the numerous transition metals, iron is widely used for PS activation because it is comparatively cheap, effective, non-toxic and environmentally friendly [17,20,21]. However, a shortcoming to the homogeneous catalysis involving instantaneous completion of reaction is the rapid oxidation of  $\text{Fe}^{2+}$  to  $\text{Fe}^{3+}$ , which would result in inactivation of  $\text{Fe}^{2+}$  and poor utilization of PS [22,23]. In order to overcome this problem, heterogeneous catalysis systems have attracted a lot of attention as a promising alternative because of some advantages such as operation at ambient temperature, near-neutral pH, easy recovery and reuse of the catalysts [24–27].

As is well known, perovskite-type mixed oxides with general formula of  $\text{ABO}_3$  are promising heterogeneous catalysts for the removal of pollutants owing to their [28] fascinating and well defined structure and intrinsic properties. The catalytic versatility of perovskites is believed to be governed by the high mobility of oxygen and the stabilization of unusual oxidation states in their structure [29]. BFO MNPs of perovskite-type structure have been considered as an attractive photocatalyst because of its narrow band gap energy (2.2 eV) as well as its high chemical stability. Furthermore, BFO MNPs was also used as heterogeneous catalyst in Fenton-like reactions for the degradation of organic pollutants [29–31]. As BFO MNPs simultaneously have Fe element and perovskite-type structure, it is anticipated that BFO MNPs are a powerful heterogeneous catalyst for the catalytic activation of PS. However, the studies on oxidation with BFO MNPs in the presence of PS remain limited.

In this study, BFO MNPs were successfully synthesized via a novel and simple sol-gel method and used as efficient activator of PS to produce  $\text{SO}_4\cdot^-$  for the degradation of aniline from aqueous solution. The main objectives of this study are to 1) synthesize and characterize BFO MNPs; 2) assess the PS activation efficiency with BFO MNPs to facilitate the degradation of aniline in aqueous solution; 3) elucidate the dominant radical species generating from PS oxidation and resulting in aniline degradation.

## 2. Experimental

### 2.1. Materials

All chemicals and reagents used in the experiments were of analytical grade. Aniline ( $\text{C}_6\text{H}_7\text{N}_2$ , > 98.0%), Bismuth nitrate ( $\text{Bi}(\text{NO}_3)_3 \cdot 5\text{H}_2\text{O}$ ), iron nitrate ( $\text{Fe}(\text{NO}_3)_3 \cdot 9\text{H}_2\text{O}$ ), 5, 5-Dimethyl-1-pyrroline N-oxide (DMPO, AR, P96.0%) were purchased from Aladdin Reagents Co. Ltd. (Shanghai, China). Ethanol (EtOH), *tert*-butyl alcohol (TBA) were purchased from Shanghai Reagents Co. Ltd. (Shanghai, China). Sodium thiosulfate pentahydrate ( $\text{Na}_2\text{S}_2\text{O}_3 \cdot 5\text{H}_2\text{O}$ , > 99.0%) was obtained from Guangzhou Chemical Reagents Factory

(Guangzhou, China).  $\text{Na}_2\text{S}_2\text{O}_8$ , concentrated sulfuric acid ( $\text{H}_2\text{SO}_4$ , > 98.0%) and sodium hydroxide ( $\text{NaOH}$ , > 96.0%) were purchased from Tianjin Baishi Chemical Reagents Co. Ltd. (Tianjin, China). Water used in this study was deionized distilled water produced by a Millipore Milli-Q system (USA).

### 2.2. Synthesis of BFO MNPs

BFO MNPs were synthesized by a simple sol-gel process as reported previously [30]. For the synthesis of BFO MNPs, the equal mole concentration of Bismuth nitrate (0.008 mol) ( $\text{Bi}(\text{NO}_3)_3 \cdot 5\text{H}_2\text{O}$ ) and Iron nitrate ( $\text{Fe}(\text{NO}_3)_3 \cdot 9\text{H}_2\text{O}$ ) (0.008 mol) were dissolved in 20 ml of 2-methoxyethanol, followed by adding 20  $\mu\text{l}$  of  $\text{HNO}_3$  (0.1 mol/L). After the addition of citric acid (0.008 mol) and ethylene glycol (10 ml) to the solution, the mixture was stirred for 1 h at 60 °C to form a sol. The sol was heated for 5 h at 100 °C to form a brown viscous resin. The resin was heated for 5 min on an electric furnace, and then calcined at 500 °C for 2 h.

### 2.3. Characterizations

The surface morphology of BFO MNPs was observed with EVO 18 (Car Zeiss) scanning electron microscope (SEM) being operated at an acceleration voltage of 10 kV. The crystalline structure was characterized by X-ray diffractometer (XRD, D8 Advance, Bruker) with  $\text{Cu K}\alpha$  radiation ( $\lambda = 1.541 \text{ nm}$ ) over a  $2\theta$  range of 10°–80°. The valence state of elements was determined by X-ray photoelectron spectroscopy (XPS) Phi X-tool instrument. The infrared spectra were recorded on a Fourier transform infrared (FTIR) spectrophotometer. The spectra were obtained from 400 to 4000 wave numbers ( $\text{cm}^{-1}$ ) using a Vector 33 (Bruker, German).

### 2.4. Experimental process

Aniline and PS stock solutions with concentrations of 10 mM and 50 mM, respectively, were prepared with deionized water. All experiments were performed in 250 ml Erlenmeyer flasks under constant stirring in a rotary shaker at 25 °C and 125 rpm. For aniline degradation experiments, predetermined amount of catalyst was added into 100 ml of 0.5 mM aniline solution and followed by adding 5 mM PS solution at pH 7.0. The initial pH of aniline solution was adjusted by 0.1 M  $\text{H}_2\text{SO}_4$  and 0.1 M  $\text{NaOH}$ . At regular time intervals, 0.5 ml sample was taken and filtered through 0.22  $\mu\text{m}$  syringe filters prior to analysis. After filtration samples were quenched immediately with sodium thiosulfate to stop the reaction. Various parameter effects on aniline degradation, including dosage of catalyst, solution of pH, and PS concentration of the aniline solution were investigated. All these experiments were performed in triplicate.

### 2.5. Analytical methods

The concentration of aniline in the aqueous phase was measured by High Performance Liquid Chromatography (HPLC) (Shimadzu LC-20) equipped with a diode array detector set at 254 nm. The HPLC column used was a reversed-phase  $\text{C}_{18}$  column (250 mm  $\times$  4.6 mm) and the temperature of the column was maintained at 40 °C. The mobile phase used was methanol–water (70: 30, v/v) with a flow rate at 0.7  $\text{ml min}^{-1}$ . Persulfate anion concentration was determined by spectrophotometric method with potassium iodide [32]. GC–MS Varian 4000 GC–MS (gas chromatography–mass spectrometry) with a weak polarity capillary column ((0.15 lm) 60 m 0.25 mm) was used to verify the structure of the intermediates. The mineralization of aniline was determined by EMENTAR LiquiTOC Total Organic Carbon (TOC) analyzer. An electron paramagnetic resonance spectrometer (EPR) (Bruker, A300 microx) was used to determine the generation of sulfate and hydroxyl radicals. DMPO (0.1 M) was used as the radical spin-trapping

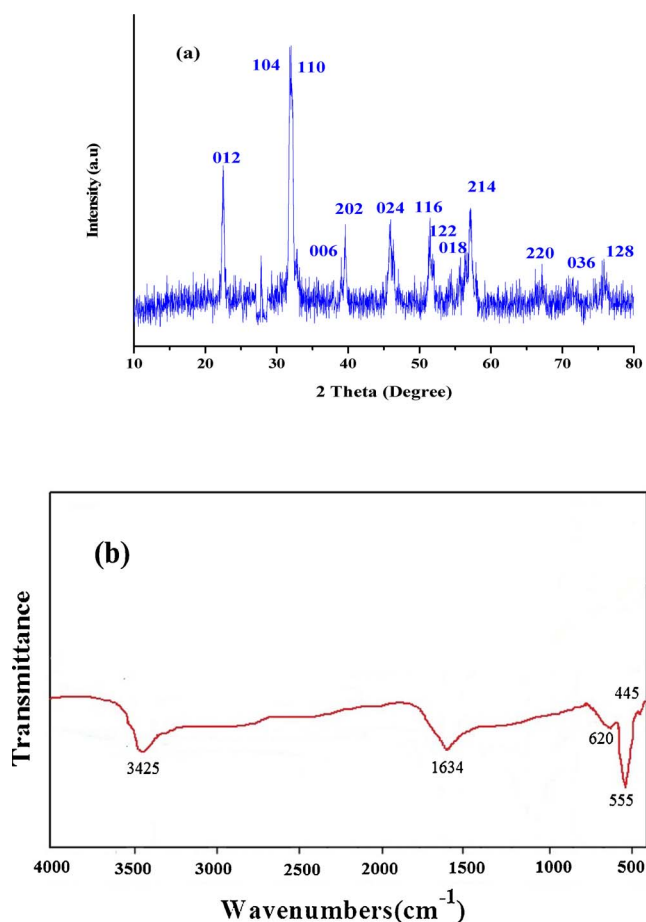


Fig. 1. XRD patterns (a) and FT-IR spectra (b) of BFO MNPs.

reagent. The EPR determination was performed under the following conditions: a center field of 3517 G, a microwave power of 20.16 mW, a microwave frequency of 9.875 GHz, a sweep width of 250 G, a modulation frequency of 100 kHz, a receiver gain of  $3.99 \times 10^4$ , modulation amplitude of 1.00 G, a sweep time of 122.8 s.

### 3. Results and discussion

#### 3.1. Characterization of BFO MNPs

The as-prepared BFO MNPs were first characterized by powder X-ray diffraction (XRD) measurements. The XRD pattern presented in Fig. 1a demonstrate the crystalline phase of BFO MNPs. The peaks in the XRD pattern were corresponded to the rhombohedral perovskite structure of BFO MNPs with R3c space group (JCPDS NO: 86–1518). The result of XRD data is in good agreement with those reported in literature for BiFeO<sub>3</sub> [33,34]. The crystalline size of BFO MNPs according to the (012) diffraction peak was measured by using Scherrer's formula  $d = k\lambda/\beta \cos \theta$ , where  $d$  = crystallite size,  $k = 0.9$  (shape factor),  $\lambda$  = wavelength of Cu K $\alpha$  (1.5406 Å),  $\beta$  = full width at half-maximum (fwhm), and  $\theta$  = Bragg's angle [35]. The crystalline size of BFO MNPs was found to be 60.48 nm. The FT-IR spectra of the BFO MNPs is depicted in Fig. 1b. In the FT-IR spectra of BFO MNPs, three strong absorption peaks detected around 445 cm<sup>-1</sup>, 555 cm<sup>-1</sup> and 620 cm<sup>-1</sup> were attributed to O–Fe–O bending vibrations, the Fe–O stretching of FeO<sub>6</sub> groups and bending vibration of Fe–O bond in FeO<sub>6</sub> octahedral unit in perovskite BFO, respectively. The perovskite structure formation can be confirmed by the existence of metal oxygen band. The broad band at 3425 cm<sup>-1</sup> is ascribed to the bond stretching in H<sub>2</sub>O and –OH groups. While the band around 1634 cm<sup>-1</sup> can be attributed

to the bending vibrations of the H<sub>2</sub>O molecules on the surface of BFO MNPs [30,33]. The characteristic scanning electron micrograph (SEM) of BFO MNPs was shown in Fig. 2a. It was found that BFO MNPs displayed a structure with particle size range of nanoscale. It is clearly revealed that BFO MNPs were observed to be wafer-like in shape that also show high porous structure. As shown in Fig. 2b, the energy-dispersive X-ray spectroscopy (EDS) analysis of BFO MNPs approved the existence of Bi, Fe and O. The quantitative analysis showed that molar ratio of Bi, Fe and O in BFO MNPs was about 1:1:3.

XPS analysis was carried out to observe the chemical states and surface compositions of BFO MNPs. As it can be seen from Fig. 3a, the two peaks around 158.9 and 164.4 eV correspond to the binding energy of Bi 4f<sub>7/2</sub> and Bi 4f<sub>5/2</sub>, respectively. The peaks confirmed the presence of

Bi<sup>3+</sup> in the BFO MNPs [36]. Fig. 3b showed the XPS pattern of Fe element, in which the binding energy of 723.8 and 710.4 eV corresponded to Fe 2p<sub>1/2</sub> and Fe 2p<sub>3/2</sub>, respectively, certified the characteristics of Fe<sup>3+</sup> [33]. The peak observed at 529.6 eV corresponding to the binding energy of O 1s in BFO MNPs for Fe–O bond (Fig. 3c) [34].

#### 3.2. Degradation of aniline under different systems

To assess the catalytic efficiency of synthesized BFO MNPs, experiments were conducted to compare aniline degradation by different treatment systems, including only BFO MNPs, only Fe<sub>3</sub>O<sub>4</sub>, only PS, Fe<sub>3</sub>O<sub>4</sub>/PS, and BFO MNPs/PS. The results showed that the removal efficiency of aniline was 13.31% and 10% in BFO MNPs and Fe<sub>3</sub>O<sub>4</sub> system, respectively (Fig. 4a). It showed that low removal efficiency of aniline could be due to adsorption on the surface of catalysts. As shown in Fig. 4a, 35.5% aniline removal was observed in PS system due to small generation of SO<sub>4</sub>·<sup>-</sup>. It can be seen that degradation efficiency obtained by PS was higher than that of BFO MNPs and Fe<sub>3</sub>O<sub>4</sub> alone, which is mainly due to generation of SO<sub>4</sub>·<sup>-</sup>. However, the results indicate that the direct aniline degradation by PS and its adsorption by BFO MNPs and Fe<sub>3</sub>O<sub>4</sub> is limited. As revealed in Fig. 4b, PS consumptions percentage was 16.4% after 120 min reaction in PS alone system, showing that small amount of PS was decomposed in this condition. At ambient temperature PS is stable and chemical reaction is slow, so a little degradation of aniline was observed. Fig. 4a also shows a higher degradation efficiency of aniline (54.25%)

for Fe<sub>3</sub>O<sub>4</sub> in the presence of PS, which was significantly greater than BFO MNPs, Fe<sub>3</sub>O<sub>4</sub> and PS each alone. This suggests that the catalytic activity was enhanced by the addition of PS to the reaction. As can be seen, when aniline in the aqueous solution was exposed to the combination of BFO MNPs and PS, the degradation efficiency of aniline was

noticeably increased and reached 100% after 120 min reaction. As displayed in Fig. 4a, for BFO MNPs/PS system aniline content was decreased much faster at initial times, indicating that the catalyst acted as an excellent activator of PS. The findings shown that BFO MNPs

catalyst has a significant effect on PS decomposition with consequent generation of SO<sub>4</sub>·<sup>-</sup>. While PS consumption was 78.3% and 38.45% in BFO MNPs/PS and Fe<sub>3</sub>O<sub>4</sub>/PS system, respectively. Aniline degradation efficiency in BFO MNPs/PS system was higher than other systems due to generation of more SO<sub>4</sub>·<sup>-</sup>. The result demonstrated that in the BFO MNPs/PS system, BFO MNPs could effectively activate PS to produce SO<sub>4</sub>·<sup>-</sup> and then hydroxyl radical would be generated by the reaction between SO<sub>4</sub>·<sup>-</sup> and H<sub>2</sub>O (Eq. (4)) [37].

#### 3.3. Effect of BFO MNPs and PS dosage on aniline degradation

In the BFO MNPs/PS system, BFO MNPs was used as the catalyst for PS activation to generate the SO<sub>4</sub>·<sup>-</sup>. Hence, the generation of SO<sub>4</sub>·<sup>-</sup> can be affected by the dosage of catalyst. In BFO MNPs/PS heterogeneous system, the degradation efficiency and rate was generally controlled by the production of SO<sub>4</sub>·<sup>-</sup>, by optimizing the dosage of BFO

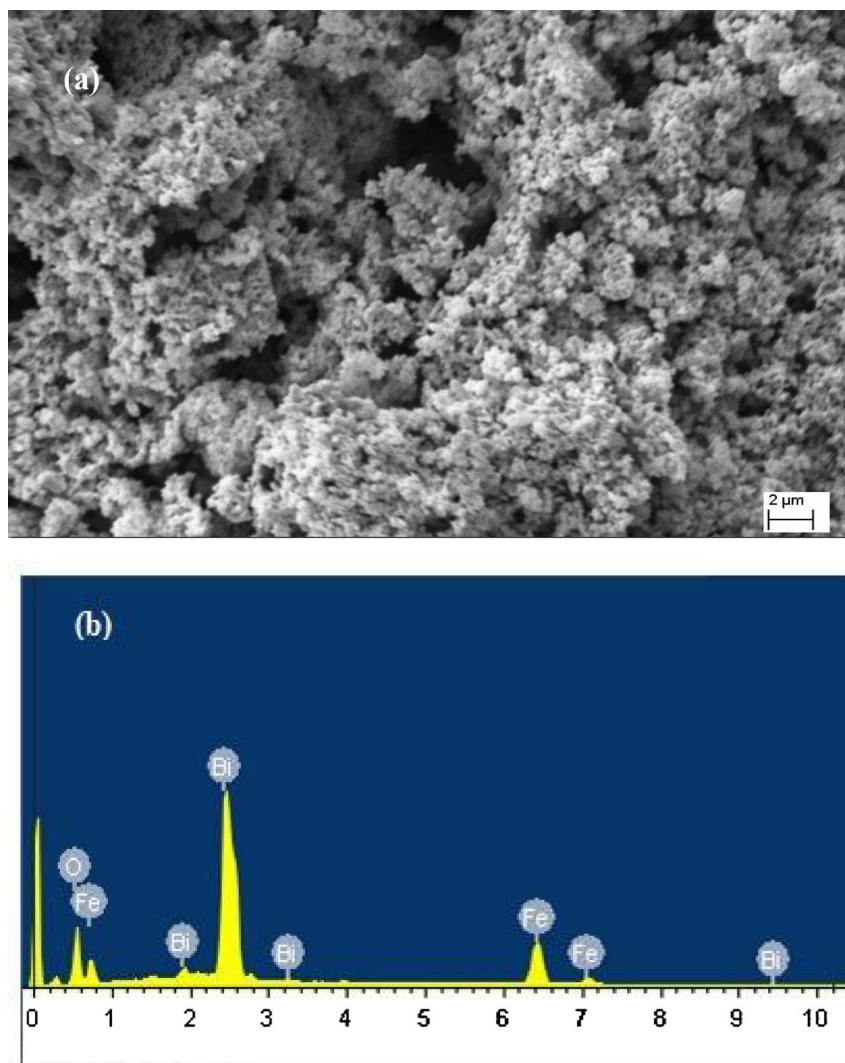


Fig. 2. SEM image of BFO MNPs (a) and (b) EDS of BFO MNPs.

MNPs. Owing to the key role of the catalyst for aniline degradation with PS, aniline kinetic study with BFO MNPs was first conducted. In order to investigate the effect of catalyst dosage on aniline degradation efficiency, experiments were conducted by different catalyst dosage in the range of 0.1–1.0 g/L. The initial aniline concentration was fixed at 0.5 mM, persulfate concentration was 5 mM and initial pH was 7.0. As can be seen, aniline degradation efficiency increased significantly with the dosage of BFO MNPs.

As shown in Fig. 5a, aniline degradation increased rapidly from 63.2% to 100% within 120 min with increasing dosage of BFO MNPs from 0.1 to 0.5 g/L. The results showed that complete degradation of aniline can be attained after 120 min oxidation reaction. Aniline degradation increased when BFO MNPs dosage was increased due to more generation of sulfate radical. Overall, the increase of BFO MNPs dosage would increase adsorption sites as well as active sites for PS activation to generate more  $\text{SO}_4^{\cdot -}$  [38] and therefore would lead to a significant increase of aniline degradation rate. By increasing the dosage of BFO MNPs from 0.5 g/L to 1.0 g/L, the total active sites on the surface of catalyst increase but the degradation of aniline was decreased to 85.7%. The reason is that the amounts of active sites on the surface of 0.5 g/L BFO MNPs have been enough with PS concentration of 5.0 mM and the equilibrium of adsorption/desorption has been attained between aniline and BFO MNPs nanoparticles [39,40]. Hence, the optimum BFO MNPs dosage was selected as 0.5 g/L in the following experiments.

To further investigate the removal of aniline with various BFO

MNPs dosage, pseudo-first order kinetics model was used to fit the catalytic results under various BFO MNPs dosage. The kinetics model can be expressed as  $\ln C/C_0 = -kt$ , where  $C$  and  $C_0$  are aniline concentrations (mM) at time  $t$  and time zero, respectively,  $k$  is the pseudo first order degradation rate constant ( $\text{min}^{-1}$ ). The degradation of aniline in all conditions followed the pseudo first order kinetic model well ( $R^2 > 0.98$ ). The apparent rate constants of aniline increased from 0.0113 to 0.0332  $\text{min}^{-1}$

with increasing dosages of BFO MNPs from 0.1 to 0.5 g/L and it decreased to 0.0258  $\text{min}^{-1}$  with increasing dosage of catalyst from 0.5 g/L to 1.0 g/L as shown in Fig. 5b. As depicted in Fig. 5b, aniline degradation well followed pseudo-first order model ( $R^2 > 0.98$ ). The results also demonstrated that the degradation efficiency was the highest at a BFO MNPs dosage of 0.5 g/L.

The concentration of oxidant is a main factor that can significantly affect the degradation of

organic pollutants. Initial concentration of PS can play a significant role as an oxidizing agent in the system due to the production of more amount of  $\text{SO}_4^{\cdot -}$ . It can be seen from Fig. 5c that rate constant of aniline degradation increased from 0.0069 to 0.0332  $\text{min}^{-1}$  when the concentration of PS was increased from 0.5 to 5.0 mM, but rate constant decreased to 0.0276  $\text{min}^{-1}$  when the concentration of PS was further increased to 10 mM. Aniline degradation efficiency increased and reached at 100% when the concentration of PS was increased to 5 mM. With the increasing PS concentration, more molecules of PS could reach

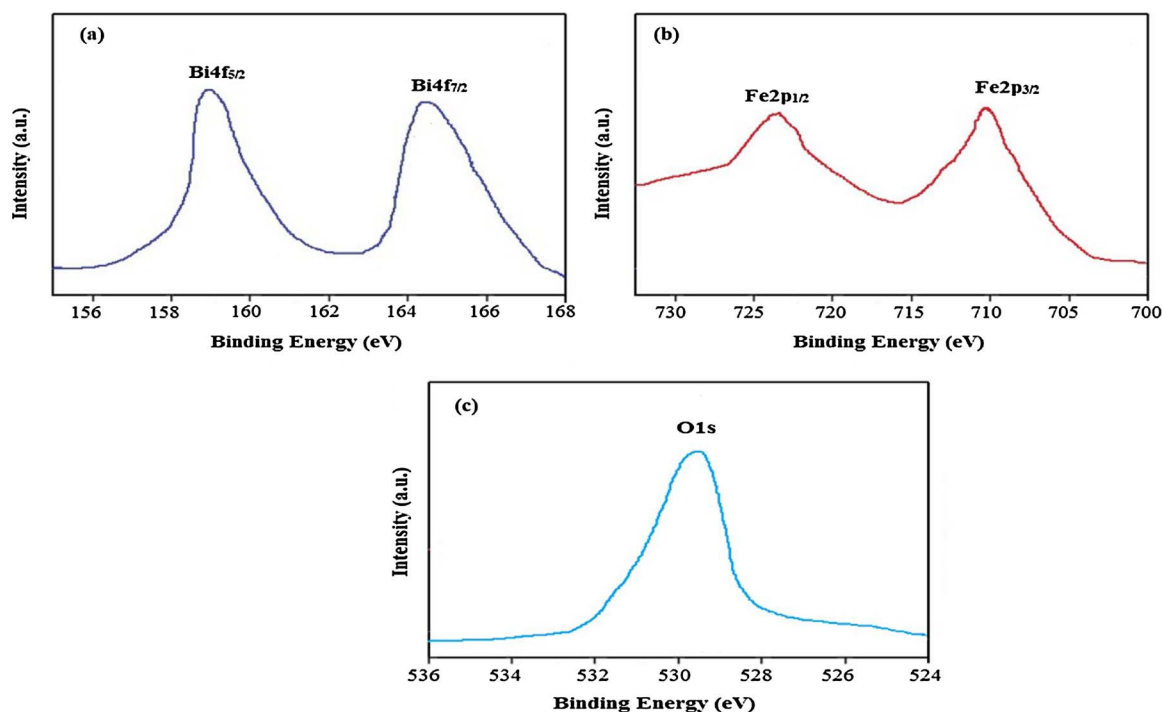


Fig. 3. XPS spectra of BFO MNPs (a) Bi 4f, (b) Fe2p, and (c) O 1s.

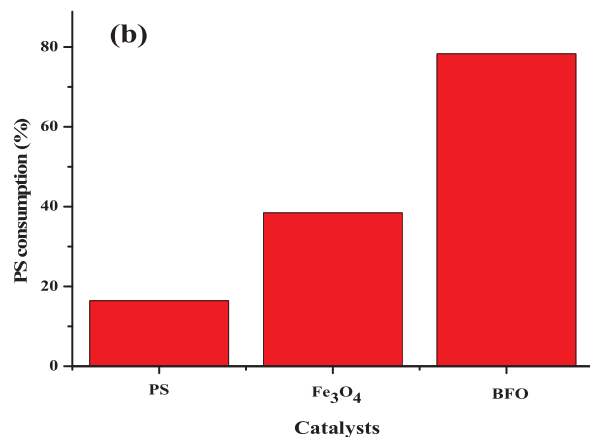
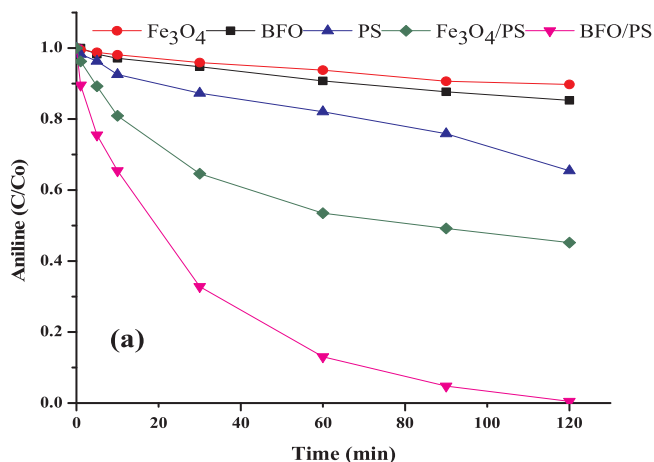


Fig. 4. Degradation of aniline in different systems (a); [aniline] = 0.5 mM; [BFO] = 0.5 g/L; [Fe<sub>3</sub>O<sub>4</sub>] = 0.5 g/L [PS] = 5.0 mM; Temp = 25 °C; pH = 7.0; (b) consumption of PS.

the surface of BFO MNPs and then react with Fe<sup>2+</sup>, large amounts of SO<sub>4</sub><sup>•-</sup> were produced due to the higher concentration of PS, which resulted in enhanced aniline degradation. In agreement with previous studies [41,42], it was found PS activation with Fe<sup>2+</sup> could result in degradation of other contaminants from aqueous solution. However, the excessive PS concentration (10 mM) cannot increase the degradation efficiency of aniline. Therefore, aniline degradation rate of 95.2% was obtained after 120 min. SO<sub>4</sub><sup>•-</sup> scavenging effect was elucidated by three processes, (a) SO<sub>4</sub><sup>•-</sup> consumption with excess PS (Eq. (6)), (b) the presence of an unproductive PS decomposition reaction (without generation of SO<sub>4</sub><sup>•-</sup>) and (c) excess SO<sub>4</sub><sup>•-</sup> recombination and annihilation (Eq. (7)) [43]. Hence, excessive presence of PS reacting with BFO MNPs to degrade aniline, PS competed with aniline for SO<sub>4</sub><sup>•-</sup> which resulted in decreased degradation efficacy. [44,45].



#### 3.4. Effect of initial pH on aniline degradation

pH is one of the most important parameters that influence the degradation of organic pollutants. The experiments were conducted at different pH 3.0, 5.0, 7.0, 9.0 and 11.0 to investigate the effect of initial pH on aniline degradation. The initial aniline concentration was fixed at 0.5 mM, PS concentration was 5.0 mM and catalyst dosage was 0.5 g/L. The results showed that pH significantly influenced the degradation efficiency of aniline. Aniline degradation efficiency declined with increasing solution pH (Fig. 6). As depicted in Fig. 6, aniline degradation was 100% at pH 3.0 and pH 5.0 within 10 min and 30 min, respectively. This is because BFO MNPs can more easily activate PS under acidic condition to produce more SO<sub>4</sub><sup>•-</sup> on the catalyst surface. When pH increased from 3.0 to 11.0 during 120 min of reaction, the degradation efficiency of aniline decreased from 100% to 57.61%. At pH 7.0, 9.0 and 11.0, aniline removal after 120 min reaction time was 100%, 78.22% and 57.61%, respectively. The order of aniline degradation efficiencies was pH 3.0 > pH 5.0 > pH 7.0 > pH 9.0 > pH 11.0. Under acidic conditions, more SO<sub>4</sub><sup>•-</sup> could be generated because of

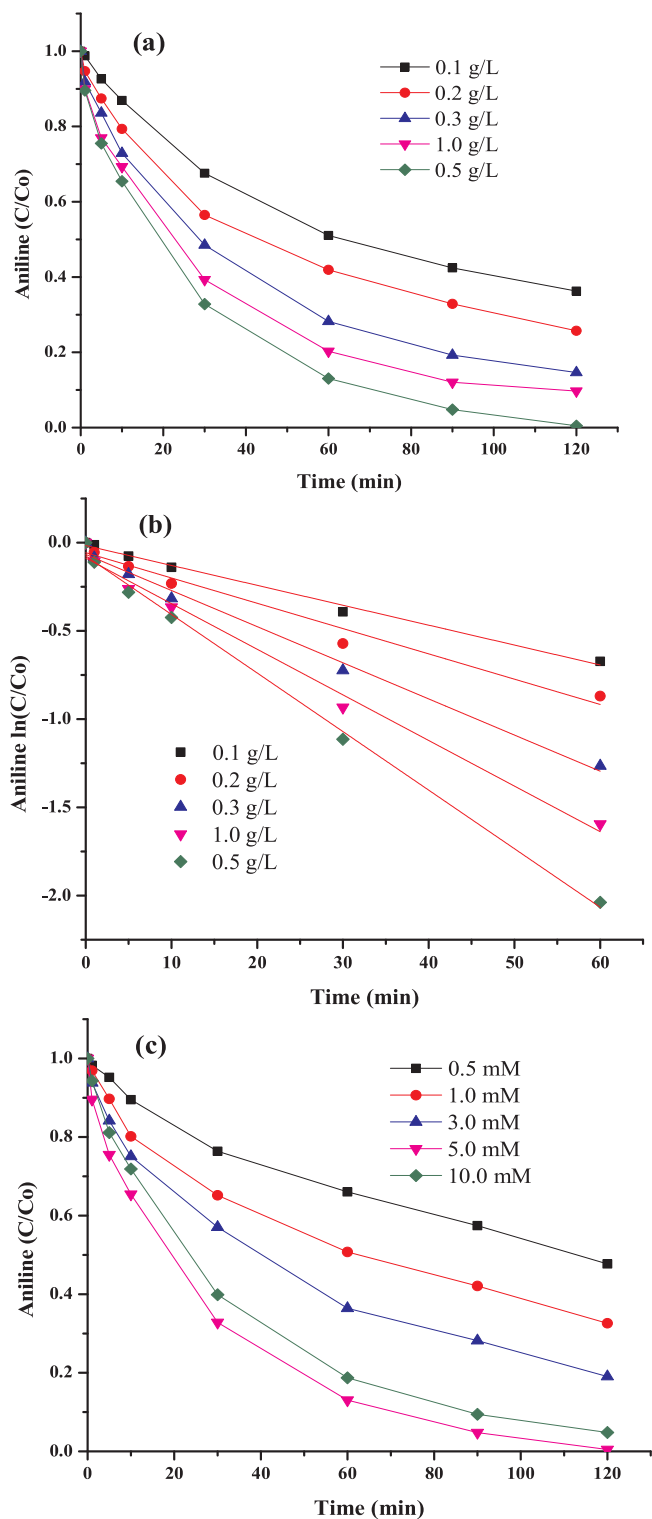


Fig. 5. (a) Effect of BFO MNPs dosage on the degradation of aniline; (b) Pseudo-first order kinetics fitting data for the degradation of aniline; (c) Effect of PS concentrations on the degradation of aniline; [aniline] = 0.5 mM; [PS] = 5.0 mM; Temp = 25 °C; pH = 7.0.

further acid catalyzed (Eqs. (8), (9)) [46,47]. Aniline degradation increased due to the production of more  $\text{SO}_4^{\cdot-}$  and complete degradation of aniline was achieved.

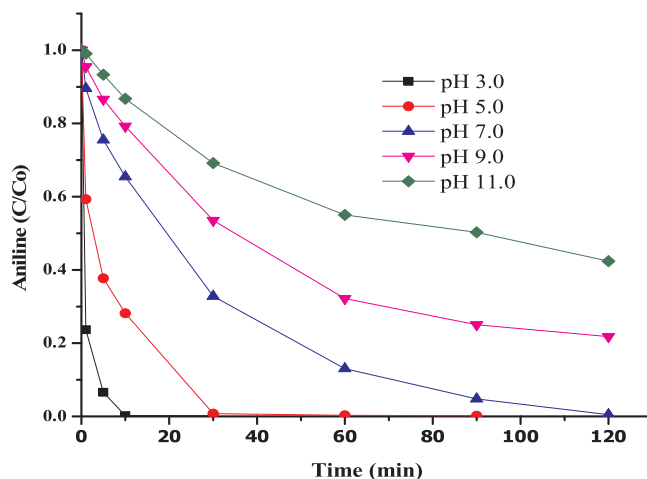


Fig. 6. Effect of initial pH on the degradation of aniline; [aniline] = 0.5 mM; [PS] = 5.0 mM; Temp. = 25 °C; [BFO MNPs] = 0.5 g/L.

On the other hand, under basic conditions  $\text{SO}_4^{\cdot-}$  would directly convert into  $\cdot\text{OH}$  through the reaction with water and  $\text{OH}^-$  (Eqs. (4), (5)) [48]. Though  $\cdot\text{OH}$  exert a higher redox potential than

$\text{SO}_4^{\cdot-}$ , the accompanying production of abundant  $\text{SO}_4^{2-}$  may prevent the reactivity of  $\text{SO}_4^{\cdot-}$  and  $\cdot\text{OH}$ . Simultaneously,  $\text{Fe}(\text{OH})_2$  or ferric hydroxide complexes such as  $\text{Fe}(\text{OH})_2^{4+}$ ,  $\text{Fe}(\text{OH})^{2+}$ ,

$\text{Fe}(\text{OH})_3$  and  $\text{Fe}(\text{OH})_4^-$  would be produced and cover the surface of catalyst [6].  $\text{Fe}(\text{OH})_2$  or ferric hydroxide complexes have much lower or no catalytic activity for PS activation. Moreover, the generation of ferric hydroxide complexes would lead to iron hydroxides adsorption on the surface of BFO MNPs, which prevented  $\text{Fe}^{2+}$  release and PS activation with  $\equiv\text{Fe}^{\text{II}}$  on the surface of catalyst [49]. Furthermore, as shown in Fig. 6, aniline degradation efficiency at pH 7.0 is 100%. The finding of this study suggests that BFO MNPs/PS system shows a respectable catalytic activity toward aniline degradation without using acid conditions. These results also demonstrated that BFO MNPs/PS system could be effectively used over a wide pH range.

### 3.5. Effect of temperature on aniline degradation

To explore the effect of the reaction temperature on the degradation of aniline, experiments were conducted at 15 °C, 25 °C and 35 °C. The results demonstrated that the reaction temperature has a significant effect on aniline degradation (Fig. 7). Aniline degradation efficiency remarkably increased with increasing temperature. As shown in Fig. 7, the performance of BFO MNPs for PS activation was increased at elevated temperature. For example 75.12% and 100% of aniline was degraded after 120 min at 15 °C and 25 °C, respectively. While, 100% aniline degradation was achieved within 60 min at 35 °C. This was because of enhanced generation of  $\text{SO}_4^{\cdot-}$  in BFO MNPs/PS system due to PS activation by heat and catalyst and results in rapid degradation of aniline in aqueous solution. The results also revealed that aniline degradation followed the pseudo-first-order kinetic model. The degradation rate constants of aniline at 15 °C, 25 °C and 35 °C were calculated to be 0.0113, 0.0332, 0.1134  $\text{min}^{-1}$ , respectively. Moreover, the activation energy for aniline degradation was determined based on the pseudo-first-order rate constants by using Arrhenius equation,  $\ln k = \ln A - E_a/RT$  [41], where R is the universal gas constant (8.314  $\text{J mol}^{-1} \text{K}^{-1}$ ), A is the pre-exponential factor,  $E_a$  is the apparent activation energy, and T is the absolute temperature. The value of activation energy of the reaction was calculated to be 17.9  $\text{kJ mol}^{-1}$ .

### 3.6. Mechanistic insights

It has been revealed that PS can be activated by catalysts to produce

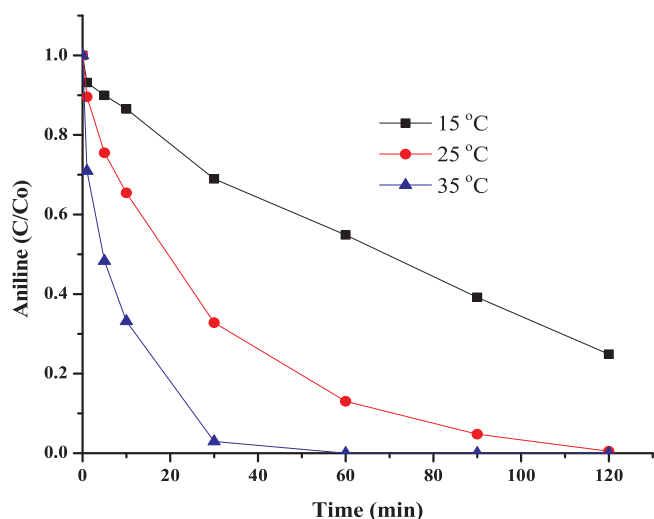


Fig. 7. Effect of temperature on the degradation of aniline; [aniline] = 0.5 mM; [PS] = 5 mM; [BFO MNPs] = 0.5 g/L; pH = 7.0.

$\text{SO}_4^{\cdot-}$  and  $\cdot\text{OH}$  [50]. In order to assess aniline degradation mechanism in BFO MNPs/PS system, quenching experiments were performed to check whether  $\text{SO}_4^{\cdot-}$  and  $\cdot\text{OH}$  were responsible for the observed degradation of aniline. Two kinds of alcohols, ethanol (EtOH, containing  $\alpha$ -hydrogen) and *tert*-butyl alcohol (TBA, without  $\alpha$ -hydrogen) were used to examine the roles of  $\text{SO}_4^{\cdot-}$  and  $\cdot\text{OH}$  for the degradation of aniline [51,52]. EtOH is an effective scavenger for both  $\text{SO}_4^{\cdot-}$  and  $\cdot\text{OH}$  and the reaction rate constants of EtOH with  $\text{SO}_4^{\cdot-}$  and  $\cdot\text{OH}$  are  $1.6\text{--}7.7 \times 10^7 \text{ M}^{-1}\text{s}^{-1}$  and  $1.2\text{--}2.8 \times 10^9 \text{ M}^{-1}\text{s}^{-1}$  respectively. TBA acts as strong quenching agent for  $\cdot\text{OH}$  and has 418–1900 times higher rate constant with  $\cdot\text{OH}$  ( $3.8\text{--}7.6 \times 10^8 \text{ M}^{-1}\text{s}^{-1}$ ) than with  $\text{SO}_4^{\cdot-}$  ( $4\text{--}9.1 \times 10^5 \text{ M}^{-1}\text{s}^{-1}$ ) [45,53].

Therefore, the dominant radical species for the degradation of aniline could be well determined by addition of EtOH or TBA into in BFO MNPs/PS system. The effect of quenching agents on aniline degradation is shown in Fig. 8a. The results showed that both EtOH and TBA exerted significant inhibiting effect on the degradation efficiency of aniline. It can be seen in Fig. 8a, aniline degradation was 100% after 120 min when no quenching agent was added. Though, when 0.5 M EtOH was added in the reaction solution, the degradation of aniline decreased to 27.33% only. In contrast, when 0.5 M TBA was added, the removal efficiency of aniline was 69.44%. The removal efficiency decreased showing that  $\cdot\text{OH}$  were quenched while  $\text{SO}_4^{\cdot-}$  could still degrade aniline. The results revealed that radical quenching effect for EtOH was higher than that for TBA. It indicated that  $\text{SO}_4^{\cdot-}$  was the predominant radical for aniline degradation.

To confirm the generation of  $\text{SO}_4^{\cdot-}$  and  $\cdot\text{OH}$ , EPR using a classic radical trapping agent, 5, 5-dimethylpyrroline-N-oxide (DMPO) was employed to capture the radical species. Fig. 8b showed the hyperfine splitting constants of free radicals DMPO adduct in BFO MNPs/PS system. The signals of DMPO- $\text{SO}_4^{\cdot-}$  and DMPO- $\cdot\text{HO}$  adducts with hyperfine splitting constants were  $a\text{N} = 13.9 \text{ G}$  and  $a\text{H} = 9.7 \text{ G}$ ,  $a\text{H} = 1.45 \text{ G}$  and  $a\text{H} = 0.76 \text{ G}$  and  $a\text{N} = 15.0 \text{ G}$  and  $a\text{H} = 14.6 \text{ G}$ , respectively. The generation of  $\text{SO}_4^{\cdot-}$  and  $\cdot\text{OH}$  can be recognized by hyperfine splitting peaks of DMPO- $\text{SO}_4^{\cdot-}$  (six lines, 1:1:1:1:1:1) and DMPO- $\cdot\text{OH}$  (four lines, 1:2:2:1) [54,55]. The results showed that  $\text{SO}_4^{\cdot-}$  was a predominant radical and played a significant role in the degradation of aniline.

In the BFO MNPs/PS system,  $\equiv\text{Fe}^{\text{III}}$  species on the surface of the whole catalyst are transformed to  $\equiv\text{Fe}^{\text{II}}$  species via electron transfer reaction (Eq. (10)). Similar to the Fenton's reactions,  $\equiv\text{Fe}^{\text{III}}$  and  $\equiv\text{Fe}^{\text{II}}$  in BFO MNPs can also excite PS to generate  $\text{SO}_4^{\cdot-}$  via Eq. ((11)–(13)) [34] (the  $\equiv$ -symbol represents the iron species on the catalyst):

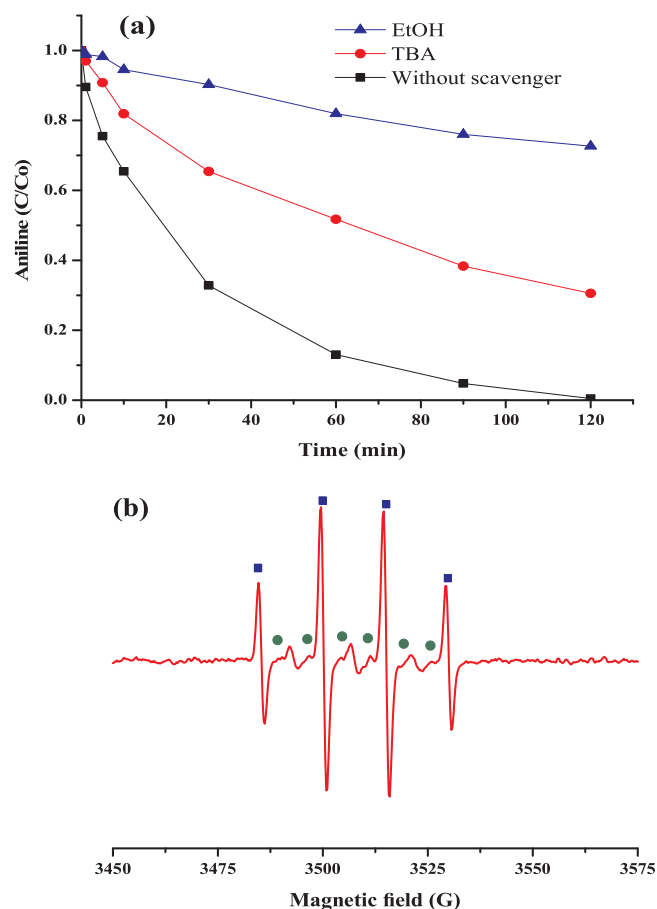


Fig. 8. (a) Effect of scavengers on the degradation of aniline; (b) EPR spectra of  $\text{SO}_4^{\cdot-}$  and  $\cdot\text{OH}$  free radical adducts at pH 7.0; [aniline] = 0.5 mM; [PS] = 5.0 mM; [BFO MNPs] = 0.5 g/L; Circles represent the DMPO- $\text{SO}_4^{\cdot-}$  and Rectangles represent the DMPO- $\cdot\text{OH}$ .



Above equations confirmed that  $\equiv\text{Fe}^{\text{II}}$  can decompose PS to generate  $\text{SO}_4^{\cdot-}$  at neutral pH. The generation of  $\cdot\text{OH}$  and the subsequent retrieval of metal ions for the purpose of catalyst reuse by Eq. (13) prevent the generation of secondary pollution. The rapid degradation of aniline with  $\text{Fe}^{2+}$ /PS duo is due to the presence of  $\equiv\text{Fe}^{\text{II}}$  species on the surface of BFO MNPs provided plentiful sources for the generation of  $\text{SO}_4^{\cdot-}$  in aqueous solution. The generated  $\text{SO}_4^{\cdot-}$  and  $\cdot\text{OH}$  can cause a rapid attack on aniline by fast catalytic degradation. These results establish that aniline has higher degradation efficiency into the BFO MNPs/PS system at neutral pH. Moreover, these results have provided new information about the design of a new type of heterogeneous catalyst. Therefore, based on the above results and analysis, a proposed mechanism depended on the generation of radical and electron transfer in BFO MNPs/PS heterogeneous oxidation process for the degradation of aniline was put forwarded as shown in Fig. 9.

To further explore the aniline degradation process, the intermediates of the aniline degradation in BFO MNPs/PS system were determined by gas chromatography-mass spectrometry (GC-MS). The effective aniline degradation by  $\text{SO}_4^{\cdot-}$  and  $\cdot\text{OH}$  has been reported in our previous work [3,23]. Hussain et al. [23] detected nitrobenzene, *p*-benzoquinone and nitroso-benzene as possible intermediates of aniline degradation by  $\text{SO}_4^{\cdot-}$  and  $\cdot\text{OH}$  in ZVI-PS system. The possible

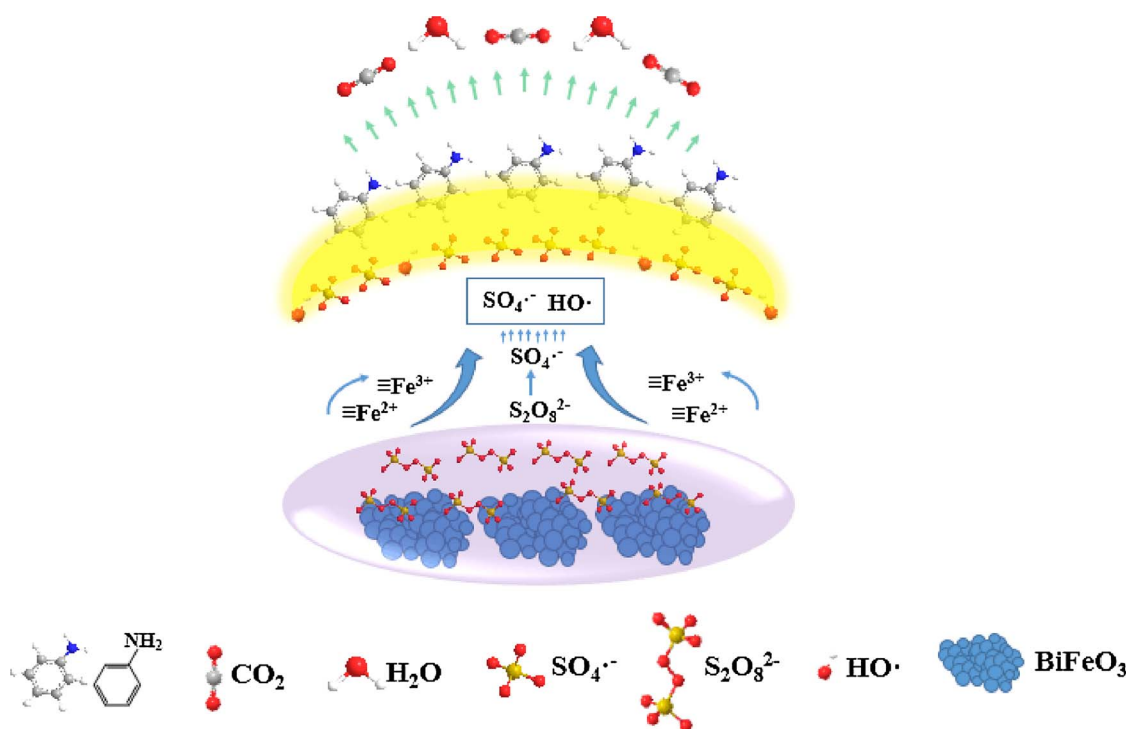


Fig. 9. Proposed mechanism of BFO MNPs/PS system.

intermediates are phenol, *p*-benzoquinone, nitrobenzene, 4-aminophenol and 4-4'-diaminodiphenyl. Therefore, based on the identified intermediates and previous work, main reaction pathways of aniline degradation are illustrated in Fig. 10. As mentioned above,  $\text{SO}_4^{\bullet -}$  and  $\cdot\text{OH}$  are main reactive oxidizing species generated by the decomposition of PS. As can be seen, aniline degradation was initiated by attack of  $\text{SO}_4^{\bullet -}$  and  $\cdot\text{OH}$  and producing 4-aminophenol and aniline radicals. The byproduct 4-4'-diaminodiphenyl was produced by the reaction of aniline radical and aniline. Then 4-4'-diaminodiphenyl was degraded to maleic acid and further mineralized to  $\text{CO}_2$  and  $\text{H}_2\text{O}$  due to its reaction with  $\text{SO}_4^{\bullet -}$  and  $\cdot\text{OH}$  [3,56]. At the same time, 4-aminophenol can be transformed into benzoquinonimine and further oxidation of benzoquinonimine by reactive oxidizing species producing *p*-benzoquinone. The degradation of nitrobenzene, as well as *p*-benzoquinone generating maleic acid and further maleic acid mineralized to  $\text{CO}_2$  and  $\text{H}_2\text{O}$ . Phenol is oxidized to hydroquinone, *p*-benzoquinone and short maleic acid which is mineralized into  $\text{CO}_2$  and  $\text{H}_2\text{O}$ .

### 3.7. Effect of anions on aniline degradation

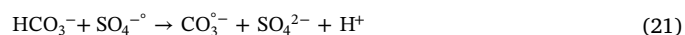
The inorganic ions are commonly present in various wastewater matrices and groundwater systems. The effect of different anions such as  $\text{NO}_3^-$ ,  $\text{Cl}^-$  and  $\text{HCO}_3^-$  on the degradation of aniline were investigated. The degradation efficiency of aniline was not affected by the addition of a low concentration of  $\text{Cl}^-$  (1 mM). However, the removal rate of aniline was decreased with the increasing concentration of  $\text{Cl}^-$ . After 120 min, 84.4% and 72% of the aniline was degraded with the addition of 5 and 10 mM  $\text{Cl}^-$ , respectively (Table 1). This may be caused by the reaction of  $\text{SO}_4^{\bullet -}$  and  $\cdot\text{OH}$  with  $\text{Cl}^-$  to generate less reactive chlorine species, which can also contribute in the degradation of aniline (Eqs. (14–17)) [55,57,58]. At lower  $\text{Cl}^-$  concentration,  $\text{Cl}^-$  reacts with  $\text{SO}_4^{\bullet -}/\cdot\text{OH}$  to produce  $\text{Cl}_2^{\bullet -}$ . But, at higher  $\text{Cl}^-$  concentration more  $\text{SO}_4^{\bullet -}/\cdot\text{OH}$  was consumed by  $\text{Cl}^-$  and  $\text{Cl}_2^{\bullet -}$  concentration quickly increased with increasing  $\text{Cl}^-$  concentration. Hence, aniline degradation efficiency was decreased.



Table 1 shows the effect of  $\text{NO}_3^-$  on aniline degradation. Aniline degradation efficiency showed no significant change with 1 mM of  $\text{NO}_3^-$ , while aniline degradation was decreased as the concentration of  $\text{NO}_3^-$  was further increased to 5.0 and 10 mM (Eqs. (18) and (19)) [55].



The inhibition effect of  $\text{HCO}_3^-$  on aniline degradation was more significant as compared to  $\text{NO}_3^-$  and  $\text{Cl}^-$ . As can be seen in Table 1, aniline degradation efficiencies were 80.3%, 71% and 60% at to  $\text{HCO}_3^-$  concentrations of 1, 5 and 10 mM respectively. The bicarbonate ions were commonly used as a radical scavenger in AOPs, thus  $\text{HCO}_3^-$  competed with aniline for reaction with  $\text{SO}_4^{\bullet -}$  and  $\cdot\text{OH}$ . Therefore,  $\text{HCO}_3^-$  quenched  $\text{SO}_4^{\bullet -}$  and  $\cdot\text{OH}$  efficiently and generated bicarbonate and carbonate radicals ( $\text{HCO}_3^{\bullet -}/\text{CO}_3^{\bullet -}$ ) with lower redox potential ( $E_0 = 1.78 \text{ V}$ ) than  $\text{SO}_4^{\bullet -}$  and  $\cdot\text{OH}$  (Eqs. (20), (21)). The reaction rate of  $\text{HCO}_3^{\bullet -}$  or  $\text{CO}_3^{\bullet -}$  with organic pollutants are two or three times lower than that of  $\text{SO}_4^{\bullet -}$  and  $\cdot\text{OH}$  [59,60]. Furthermore, the solution pH increased to basic with the addition of  $\text{HCO}_3^-$ , in which condition aniline degradation efficiency decreased.



### 3.8. Stability and reusability of BFO MNPs

The stability and reusability of catalyst is an important factor for its practical application. To assess the stability and reusability of BFO

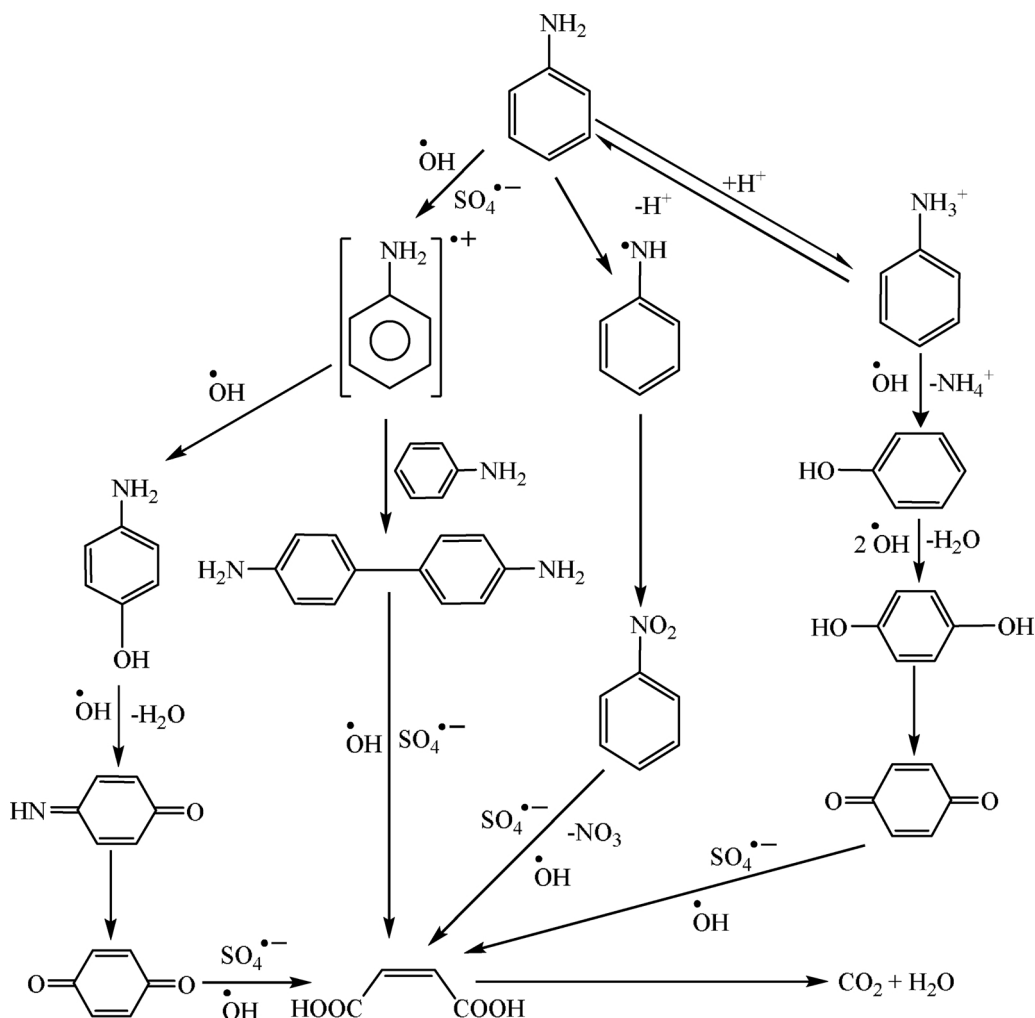


Fig. 10. Proposed possible pathways for aniline degradation in BFO MNPs/PS oxidation process.

**Table 1**  
The effect of anions on aniline degradation efficiency in the BFO MNPs/PS system.

Salts	Degradation Efficiency (%)		
Control	100		
	1 mM	5 mM	10 mM
Chloride	100	84.4	72.0
Nitrate	98.5	87.8	75.0
Bicarbonate	80.3	71.0	60.2

MNPs, experiments were conducted for five successive cycles under the following conditions of 0.5 mM aniline, 0.5 g/L BFO MNPs, 5.0 mM PS for a reaction period of 120 min. After every cycle, the catalyst was separated from the solution, washed with deionized water (3 times) and ethanol and then used for the next experiment without any modification. As can be depicted in Fig. 11, no obvious changes on aniline degradation were observed during five cycles. The results revealed that aniline degradation efficiency was 100% in the first cycle to 93.3% after five cycles of reaction. This showed that BFO MNPs catalyst is of high stability and can be reused well for the activation of PS in the catalytic oxidation process.

### 3.9. Aniline mineralization

Besides the degradation of any pollutant, the mineralization of pollutant is also another important parameter in the degradation process. In this perspective, the mineralization of aniline was analyzed by

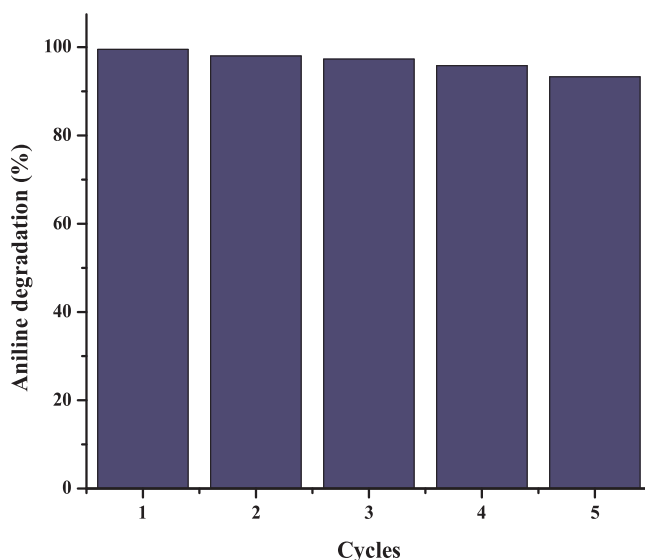


Fig. 11. Reusability study of BFO MNPs for aniline degradation; [aniline] = 0.5 mM; [PS] = 5.0 mM; Temp. = 25 °C; [BFO MNPs] = 0.5 g/L; pH = 7.0.

measuring the TOC from samples taken at regular time intervals. Fig. 12 showed aniline mineralization as a function of time at initial aniline concentration 0.5 mM, PS concentration 5 mM, pH 7.0, BFO MNPs

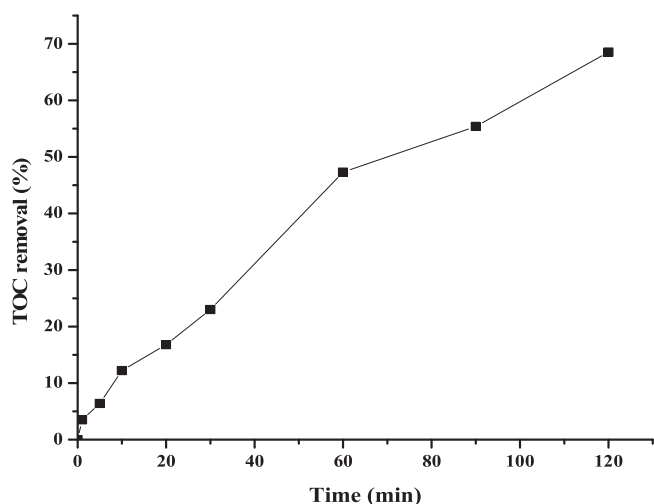


Fig. 12. TOC removal; [aniline] = 0.5 mM; [PS] = 5.0 mM; Temp. = 25 °C; [BFO MNPs] = 0.5 g/L; pH = 7.0.

dosage 0.5 g/L and a temperature of 25 °C. The results showed that BFO MNPs/PS could efficiently remove TOC from aniline solution. As depicted in Fig. 12, the mineralization efficiency of aniline was markedly increased and the removal efficiency of TOC was also increased with increasing time. The degradation efficiency of aniline was 67.18% after 30 min (Fig. 4a) while the mineralization of aniline was 23% at that time. However, the mineralization of aniline increased with passage of time and 68.55% aniline was mineralized after 120 min. The degradation of aniline was higher when compared to TOC removal efficacy under the same conditions. Aniline degradation was 100% and the removal efficiency of TOC was only 68.55%. These results proved the highly effective mineralization of aniline during degradation. Hence, both the degradation and TOC removal represented that BFO MNPs/PS system could highly enhance the catalytic performance of aniline from aqueous solution.

#### 4. Conclusions

Heterogeneous degradation of aniline from aqueous solution was examined with BFO MNPs,

which were successfully prepared via a novel and simple sol-gel method. In BFO MNPs/PS system,  $\text{Fe}^{3+}$  in the synthesized catalyst could be successfully transformed into  $\text{Fe}^{2+}$ , which activate PS to generate  $\text{SO}_4^{\cdot-}$ . As a heterogeneous activator, BFO MNPs could activate PS to a more active state, which degrade aniline and reached 100% degradation efficiency in aqueous solution after 120 min. The BFO MNPs/PS system was effective for the degradation of aniline over a wide pH range of 3.0–11.0, and the acidic pH was more favorable for aniline degradation than neutral and basic. Aniline degradation efficiency was significantly influenced by initial pH, catalyst dosage and PS concentration. Radical scavenging and EPR results revealed that both  $\text{SO}_4^{\cdot-}$  and  $\cdot\text{OH}$  were responsible for degradation of aniline. The achieved results showed that BFO MNPs have high potential for the treatment of wastewater containing various organic pollutants because of high catalytic activity, easy synthesis, stability and reusability.

#### Acknowledgements

This work was financially supported by the National Natural Science Foundation of China (51572089), the National Key Research and Development Program of China (2016YFC0400708), the Natural Science Foundation of Guangdong Province, China (2015A030313232), China Postdoctoral Science Foundation Funded Project (2016M602602) and the Foundation of Science and Technology

Planning Project of Guangdong Province, China (2016A050502007).

#### References

- [1] L. Jiang, L. Liu, S. Xiao, J. Chen, Chem. Eng. J. 284 (2016) 609–619.
- [2] A. Benito, A. Penades, J.L. Lliberia, R.G. Olmos, Chemosphere 166 (2017) 230–237.
- [3] X. Xie, Y. Zhang, W. Huang, S. Huang, J. Environ. Sci. 24 (5) (2012) 821–826.
- [4] X. Li, H. Xu, W. Yan, D. Shao, J. Electroanal. Chem. 775 (2016) 43–51.
- [5] A.R. Ribeiro, O.C. Nunes, M.F.R. Pereira, A.M.T. Silva, Environ. Int. 75 (2015) 33–51.
- [6] A.J. Jafari, B. Kakavandi, N. Jaafarzadeh, R.R. Kalantary, M. Ahmadi, A.A. Babaei, J. Ind. Eng. Chem. 45 (2017) 323–333.
- [7] S.-Y. Oh, S.-G. Kang, P.C. Chiu, Sci. Total Environ. 408 (2010) 3464–3468.
- [8] I. Hussain, Y. Zhang, S. Huang, X. Du, Chem. Eng. J. 203 (2012) 269–276.
- [9] A.M. Al-Shamsi, N.R. Thomson, Ind. Eng. Chem. Res. 52 (2013) 13564–13571.
- [10] C. Cai, Z. Zhang, H. Zhang, J. Hazard. Mater. 313 (2016) 209–218.
- [11] C.A.L. Grac, A.C. de-Velosa, S.C.A. Carlos, Catal. Today 280 (2017) 80–85.
- [12] I. Hussain, Y. Zhang, S. Huang, Q. Gao, RSC Adv. 5 (2015) 41079–41087.
- [13] A. Ghauch, A. Tuqan, Chem. Eng. J. 183 (2012) 162–171.
- [14] H. Gao, J. Chen, Y. Zhang, X. Zhou, Chem. Eng. J. 306 (2016) 522–530.
- [15] C. Tan, N. Gao, Y. Deng, W. Rong, S. Zhou, N. Lu, Sep. Purif. Technol. 109 (2013) 122–128.
- [16] W.H. Chu, D.M. Li, N.Y. Gao, M.R. Templeton, C.Q. Tan, Y.Q. Gao, Water Res. 72 (2015) 340–348.
- [17] S. Rodriguez, L. Vasquez, D. Costa, A. Romero, A. Santos, Chemosphere 101 (2014) 86–92.
- [18] Y.F. Rao, L. Qu, H.S. Yang, W. Chu, J. Hazard. Mater. 268 (2014) 23–32.
- [19] O.S. Furman, A.L. Teel, R.J. Watts, Environ. Sci. Technol. 44 (2010) 6423–6428.
- [20] S.H. Liang, C.M. Kao, Y.C. Kuo, K.F. Chen, B.M. Yang, Water Res. 45 (8) (2011) 2496–2506.
- [21] F. Vicente, A. Santos, A. Romero, S. Rodriguez, Chem. Eng. J. 170 (1) (2011) 127–135.
- [22] C.J. Liang, C.J. Bruell, M.C. Marley, K.L. Sperry, Chemosphere 55 (9) (2004) 1213–1223.
- [23] I. Hussain, Y. Zhang, S. Huang, RSC Adv. 4 (7) (2014) 3502–3511.
- [24] M. Feng, R. Qu, X. Zhang, P. Sun, Y. Sui, L. Wang, Z. Wang, Water Res. 85 (2015) 1–10.
- [25] Y. Feng, D. Wu, Y. Deng, T. Zhang, K. Shih, Environ. Sci. Technol. 50 (2016) 3119–3127.
- [26] Y. Lei, C.S. Chen, Y.J. Tu, Y.H. Huang, H. Zhang, Environ. Sci. Technol. 49 (2015) 6838–6845.
- [27] X. Duan, H. Sun, J. Kang, Y. Wang, S. Indrawirawan, S. Wang, ACS Catal. 5 (2015) 4629–4636.
- [28] F. Chi, B. Song, B. Yang, Y. Lv, S. Rana, Q. Huo, RSC Adv. 5 (2015) 67412–67417.
- [29] K. Rusevova, R. Köferstein, M. Rosell, H.H. Richnow, F.D. Kopinke, A. Georgi, Chem. Eng. J. 239 (2014) 322–331.
- [30] W. Luo, L.H. Zhu, N. Wang, H.Q. Tang, M.J. Cao, Y.B. She, Environ. Sci. Technol. 44 (2010) 1786–1791.
- [31] J.J. An, L.H. Zhu, Y.Y. Zhang, H.Q. Tang, J. Environ. Sci. 25 (2013) 1213–1225.
- [32] C.J. Liang, C.F. Huang, N. Mohanty, R.M. Kurakalva, Chemosphere 73 (2008) 1540–1543.
- [33] J. Yin, G. Liao, J. Zhou, C. Huang, Y. Ling, P. Lu, L. Li, Sep. Purif. Technol. 168 (2016) 134–140.
- [34] T. Soltani, B.K. Lee, Chem. Eng. J. 313 (2017) 1258–1268.
- [35] S. Bharathkumar, M. Sakar, S. Balakumar, J. Phys. Chem. C. 120 (2016) 18811–18821.
- [36] S. Wang, D. Chen, F. Niu, N. Zhang, L. Qin, Y. Huang, J. Alloys Compd. 688 (2016) 399–406.
- [37] S.Y. Oh, D.S. Shin, J. Chem. Technol. Biotechnol. 88 (2013) 145–152.
- [38] C. Cai, L.G. Wang, H. Gao, L.W. Hou, H. Zhang, J. Environ. Sci. 26 (2014) 1267–1273.
- [39] X. Zhang, M. Feng, R. Qu, H. Liu, L. Wang, Z. Wang, Chem. Eng. J. 301 (2016) 1–11.
- [40] J. Li, Y. Ren, F. Ji, B. Lai, Chem. Eng. J. 324 (2017) 63–73.
- [41] R. Li, X. Jin, M. Megharaj, R. Naidu, Z. Chen, Chem. Eng. J. 264 (2015) 587.
- [42] J. Yan, M. Lei, L. Zhu, M.N. Anjum, J. Zou, H. Tang, J. Hazard. Mater. 186 (2011) 1398.
- [43] S. Wang, N. Zhou, Ultrason. Sonochem. 29 (2016) 156.
- [44] G.P. Anipsitakis, D.D. Dionysiou, Environ. Sci. Technol. 38 (2004) 3705–3712.
- [45] P. Xie, J. Ma, W. Liu, J. Zou, S. Yue, X. Li, M.R. Wiesner, J. Fang, Water Res. 69 (2015) 223–233.
- [46] I. Hussain, M. Li, Y. Zhang, Y. Li, S. Huang, X. Du, G. Liu, W. Hayat, N. Anwar, Chem. Eng. J. 311 (2017) 163–172.
- [47] X. Zou, T. Zhou, J. Mao, X. Wu, Chem. Eng. J. 257 (2014) 36–44.
- [48] S.N. Su, W.L. Guo, Y.Q. Leng, C.L. Yi, Z.M. Ma, J. Hazard. Mater. 244–245 (2013) 736–742.
- [49] H. Chen, Z. Zhang, M. Feng, W. Liu, W. Wang, Q. Yang, Y. Hu, Chem. Eng. J. 313 (2017) 498–507.
- [50] Y.Q. Liu, X.X. He, Y.S. Fu, D.D. Dionysiou, Chem. Eng. J. 284 (2016) 1317–1327.
- [51] C.Y. Zhu, G.D. Fang, D.D. Dionysiou, C. Liua, J. Gao, W.X. Qin, D.M. Zhou, J. Hazard. Mater. 316 (2016) 232–241.
- [52] Y.X. Wang, L. Zhou, X.G. Duan, H.Q. Sun, E.L. Tin, W.Q. Jin, S.B. Wang, Catal. Today 258 (2015) 576–584.
- [53] J. Yan, L. Han, W. Gao, S. Xue, M. Chen, Bioresour. Technol. 175 (2015) 269–274.
- [54] G.D. Fang, J. Gao, D.D. Dionysiou, C. Liu, D.M. Zhou, Environ. Sci. Technol. 47 (2013) 4605–4611.

- [55] Y. Chen, J. Yan, D. Ouyang, L. Qian, L. Han, M. Chen, *Appl. Catal. A*. 538 (2017) 19–26.
- [56] Q. Huang, J. Zhang, Z. He, P. Shi, X. Qin, W. Yao, *Chem. Eng. J.* 313 (2017) 1088–1098.
- [57] M. Nie, C. Yan, M. Li, X. Wang, W. Bi, W. Dong, *Chem. Eng. J.* 279 (2015) 507–515.
- [58] G.D. Fang, D.D. Dionysiou, Y. Wang, S.R. Al-Abed, D.M. Zhou, *J. Hazard. Mater.* 227–228 (2012) 394–401.
- [59] J. Sharma, I. Mishra, D.D. Dionysiou, V. Kumar, *Chem. Eng. J.* 276 (2015) 193–204.
- [60] N. Jaafarzadeh, F. Ghanbari, M. Ahmadi, *Chem. Eng. J.* 320 (2017) 436–447.